# Supporting Information

## Ellwood et al. 10.1073/pnas.1421576112

### SI Methods

Net primary production was measured using the $^{14}C$ technique to label seawater (three pseudoreplicates) collected using the trace metal clean rosette in the surface mixed layer and incubated for 24 h under simulated in situ conditions (1). Picophytoplankton (phytoplankton <2 μm) and heterotrophic bacterial abundance were determined by flow cytometry (2). Microzooplankton (ciliates) were identified to genus where possible and enumerated using epifluorescence microscopy (2). Ciliate biomass estimates were obtained by converting to carbon biomass after estimation of cell volumes using algorithms (2).

### SI Results and Discussion

The concentration versus depth profiles for dissolved iron, copper and zinc (Fig. S3) show enrichment adjacent to the Brothers underwater volcano [northwest vent, vent depth ∼1,455 m (3)] consistent with other studies of the volcanoes within this region that show metal enrichment in the waters immediately surrounding the volcano, but which decrease with vertical distance away from the volcano mouth (3). Nearer the surface, at ∼1,000 m depth, dissolved iron, copper, and zinc concentrations decrease to levels consistent with background concentrations measured for the Southwest Pacific region (Fig. S3) (4, 5).


1. Boyd PW, et al. (2012) Microbial control of diatom bloom dynamics in the open ocean. *Geophys Res Lett* 39(18):L18601.
2. Hall JA, Safi K, Cumming A (2004) Role of microzooplankton grazers in the subtropical and subantarctic waters east of New Zealand. *N Z J Mar Freshwater Res* 38:91–101.
3. Massoth GJ, et al. (2003) Chemically rich and diverse submarine hydrothermal plumes of the southern Kermadec volcanic arc (New Zealand). *Geol Soc Spec Publ* 219(1): 119–139.
4. Ellwood MJ, et al. (2014) Pelagic iron cycling during the subtropical spring bloom, east of New Zealand. *Mar Chem* 160:18–33.
5. Ellwood MJ, et al. (2013) Relationships between nutrient stocks and inventories and phytoplankton physiological status along an oligotrophic meridional transect in the Tasman Sea. *Deep Sea Res Part I* 72:102–120.

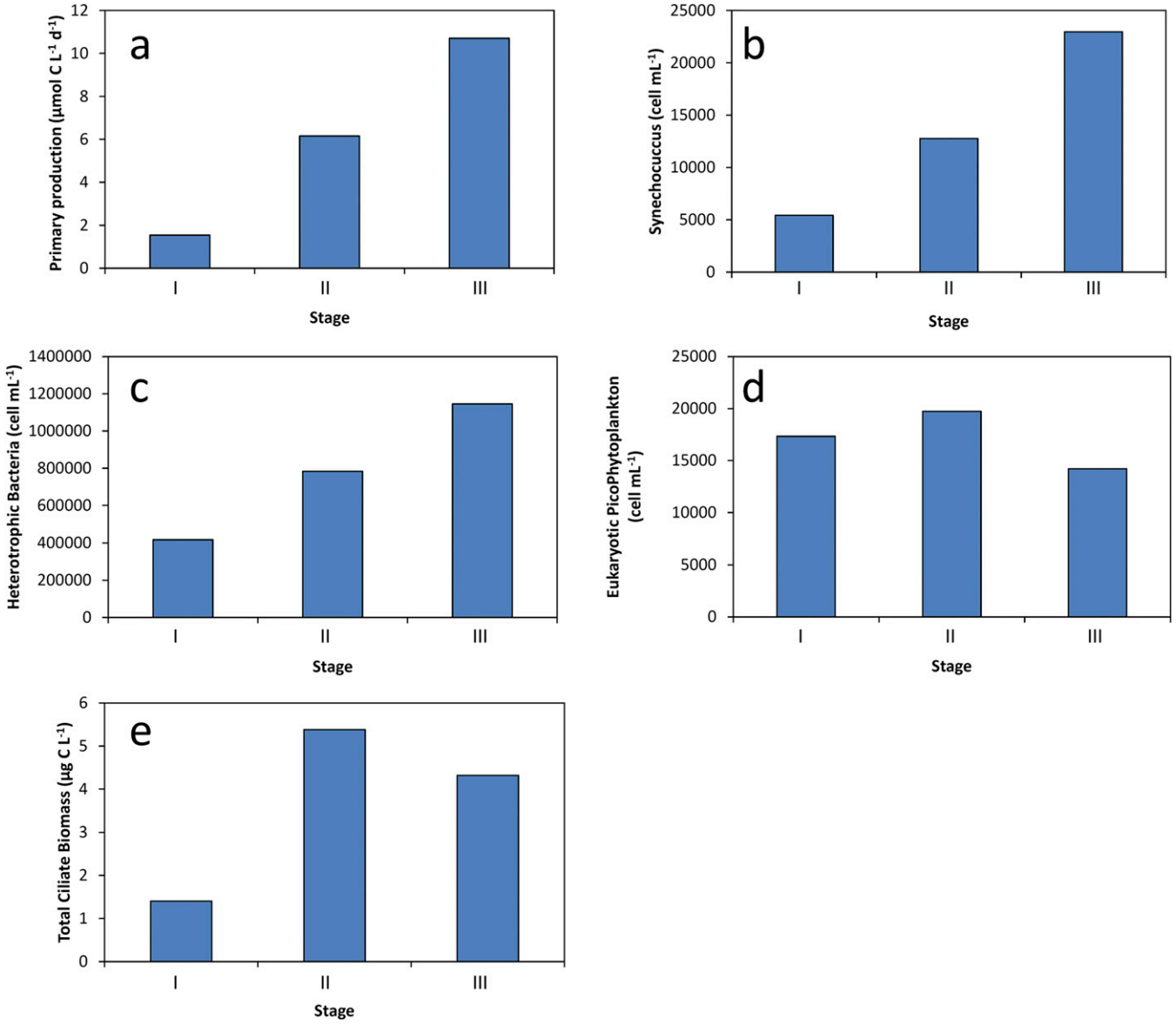


**Fig. S1.** Selected biological rates and stocks across stages I, II, and III. (*A*) Net primary production. (*B*) *Synechococcus* abundance. (*C*) Heterotrophic bacteria abundance. (*D*) Eukaryotic picophytoplankton abundance. (*E*) Total ciliate biomass.

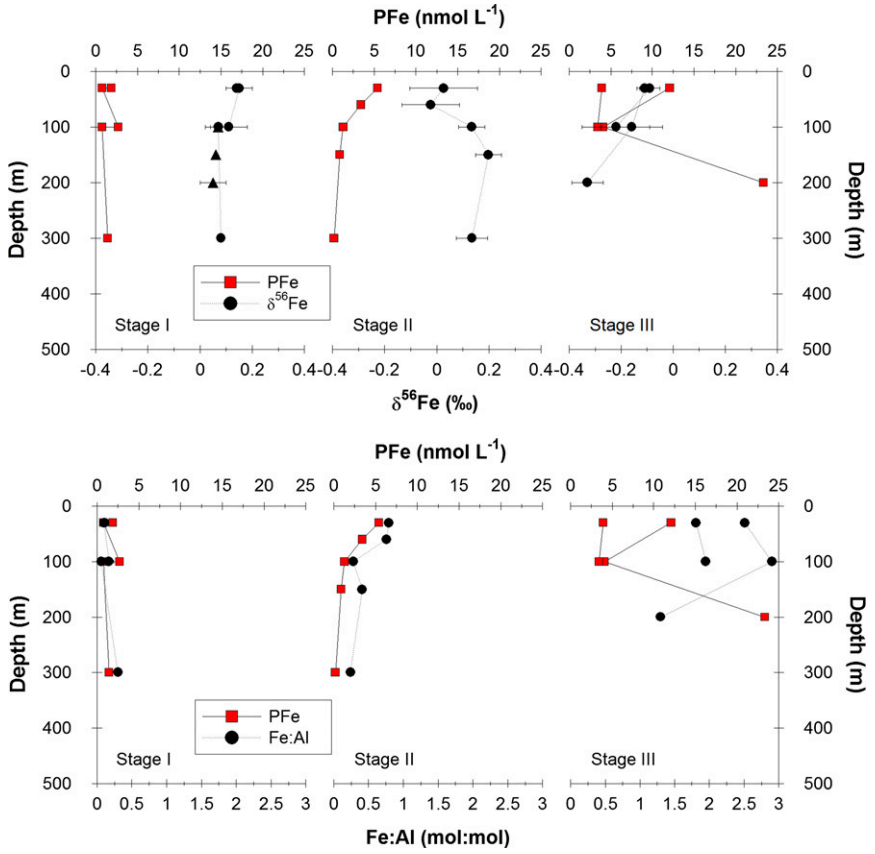


**Fig. S2.** Depth profiles of particulate iron concentrations, $\delta^{56}$Fe composition of particulates, and Fe:Al of particulates across bloom stages I, II, and III.

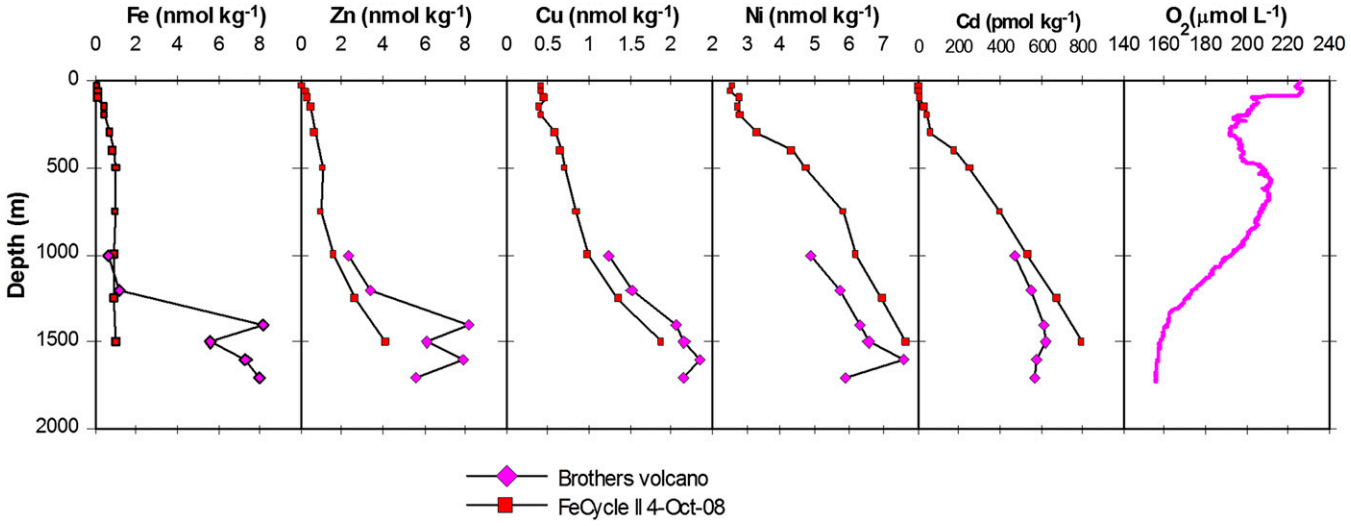


**Fig. S3.** Profiles of dissolved trace metals for the Brothers underwater volcano and the FeCycle II site. Depth profiles of dissolved iron, zinc, copper, nickel, and cadmium for samples collected adjacent to Brothers underwater volcano and at the FeCycle II site on October 4, 2008 (4). Also presented is the dissolved oxygen profile for the Brothers CTD cast.

**Table S1. Extrapolation of photochemical reduction and biological processing to the particulate iron pool**

| Process | Rate constant or flux | Flux, pmol·L$^{-1}$·d$^{-1}$ |
|---|---|---|
| Photochemical reduction of PFe to DFe | 0.018 h$^{-1}$* | DFe: 240[†] |
| | 14.4 nmol (μmol PFe) h$^{-1}$[‡] | DFe: 192[†] |
| | 16.8 nmol (μmol PFe) h$^{-1}$[‡] | DFe: 240[†] |
| | 2 pmol L$^{-1}$ h$^{-1}$[§] | DFe: 133[†] |
| Biological processing of PFe to bioavailable Fe | 0.002 h$^{-1}$* | DFe: 72[¶] |
| Biological processing of Pfe | 0.002 h$^{-1}$* | DFe: 72 |
| PFe regeneration | | |
| Stage II | | PFe: 100[#] |
| Stage III | | PFe: 160[#] |

*Rate constants taken from Barbeau et al. (1) for the release of dissolved iron from ferrihydrite.

[†]Assumes a 12:12 h day:night period and accounts for diurnal changes in irradiance across the day. The average particulate iron concentration was 1.5 nmol·L$^{-1}$ for bloom stage I (0–100 m). The 1% light level was around 100 m.

[‡]Data taken from Wells and Mayer (2) for the release of dissolved iron from ferrihydrite at a pH 8 irradiated with 300 μmol quanta m$^{-2}$·s$^{-1}$ and 2,000 μmol quanta m$^{-2}$·s$^{-1}$.

[§]Data taken from Johnson et al. (3) for the photochemical reduction of particulate iron in Equatorial Pacific waters integrated to the 0.1% light level. This flux is based on a particulate iron concentration of 0.2 nmol·L$^{-1}$. We scaled this flux to 1.5 nmol·L$^{-1}$ and accounted for diurnal variations in irradiance during bloom stage I.

[¶]The biological processing of PFe (ferrihydrite) to produce bioavailable iron based on a particulate iron concentration of 1.5 nmol·L$^{-1}$ for stage I.

[#]For comparison, we have included particulate iron regeneration rates for bloom stages II and III. We do not have particulate iron regeneration rates for stage I, but project this flux to be about 25% of the stage II flux based on differences in primary production rates and ciliate biomass between bloom stages I and II (Fig. S1 *A* and *F*). Data are taken from Boyd et al. (4) and include particulate iron regeneration associated with microzooplankton herbivory, bacterivory, mesozooplankton grazing (fecal iron), and viral lysis. The release of dissolved iron from particulate iron associated with each of these regeneration processes is unknown.

1. Barbeau K, Moffett JW, Caron DA, Croot PL, Erdner DL (1996) Role of protozoan grazing in relieving iron limitation of phytoplankton. *Nature* 380:61–64.
2. Wells ML, Mayer LM (1991) The photoconversion of colloidal iron oxyhydroxides in seawater. *Deep Sea Res. Part A* 38(11):1379–1395.
3. Johnson KS, Coale KH, Elrod VA, Tindale NW (1994) Iron photochemistry in seawater from the equatorial Pacific. *Mar Chem* 46(4):319–334.
4. Boyd PW, et al. (2012) Microbial control of diatom bloom dynamics in the open ocean. *Geophys Res Lett* 39(18):L18601.

**Table S2. Iron isotope fractionation factors**

| Isotope fractionation (alpha) factors | Symbol | Range |
|---|---|---|
| Photochemical reduction of dissolved $Fe^{III}$ | $\alpha_{hvd}$ | −2.9‰* |
| Photochemical reduction and dissolution of detrital/lithogenic Fe | $\alpha_{hvl}$ | −1.7‰[†] |
| Precipitation/Scavenging of dissolved $Fe^{III}$ | $\alpha_{scav}$ | −0.1 to −1.32‰[‡] |
| Nonreductive dissolution of detrital/lithogenic Fe | $\alpha_{diss}$ | −0.1 to −0.2‰[§] |
| Dissolved iron removal associated with biological production | $\alpha_{bio}$ | −0.13 to −0.54‰[¶] |

*This value is based on the work of Welch et al. (1) and Johnson et al. (2) and assumes that iron isotope fractionation for organically complexed iron is similar to inorganic iron. Recent work has shown that photochemical and chemical reduction of iron complexed to synthetic iron chelators, such as EDTA, can produce positive and negative isotope variations (3). Although we assume direct photochemical reduction of the dissolved iron pool ($Fe^{III}/Fe^{III}L$), indirect reduction of iron can also occur via hydrogen peroxide decomposition (4, 5).

[†]This factor is based on experimental values of −1.7‰ (−2.5‰ $\delta^{57}Fe$ converted to $\delta^{56}Fe$) for photochemical induced dissolution of goethite under acidic conditions in the presence of oxalate (6).

[‡]Our value is based on the loss of dissolved iron from solution for samples collected adjacent to the Brothers underwater hydrothermal system with sampling depths ranging between 1,000 and 1,700 m (Fig. 5) based on closed system modeling. Using this approach, we get a value of −0.67‰. We justify the use of a closed system model because it (*i*) gives a reasonably good fit ($r^2 = 0.87$) to the hydrothermal data and (*ii*) is similar to the model used by Bullen et al. (7)—they used a closed system model to explain Fe (II) oxidation followed by precipitation (7, 8). Use of an open system model to describe the hydrothermal data produced an $\alpha_{scav}$ value of −1.62‰; however, the fit to the data is not so good ($r^2 = 0.76$). Our value is larger than for the rapid precipitation of hematite (−1.32; ref. 9), but lower than for its formation under equilibrium condition (−0.05‰ to −0.3‰; refs. 7 and 8). The lower value is from Skulan et al. (9) for the formation of hematite from aqueous iron (III).

[§]This value represents nonreductive dissolution of iron minerals under equilibrium conditions (9–11).

[¶]The isotope fractionation factor associated with biological uptake was assigned a value of −0.54‰ based on the overall change in iron isotope composition between stages I through III. This is similar to the values of −0.13‰ to −0.25‰ obtained by Rudic et al. (12).


1. Welch SA, Beard BL, Johnson CM, Braterman PS (2003) Kinetic and equilibrium Fe isotope fractionation between aqueous Fe(II) and Fe(III). *Geochim Cosmochim Acta* 67(22):4231–4250.
2. Johnson CM, et al. (2002) Isotopic fractionation between Fe(III) and Fe(II) in aqueous solutions. *Earth Planet Sci Lett* 195(1-2):141–153.
3. Rosenberg AD, Hodierne CE, John SG (2013) Fe isotope fractionation during reduction of Fe(III) to Fe(II). *Mineral Mag* 77(5):2083.
4. Kwan WP, Voelker BM (2002) Decomposition of hydrogen peroxide and organic compounds in the presence of dissolved iron and ferrihydrite. *Environ Sci Technol* 36(7):1467–1476.
5. Weber L, Völker C, Schartau M, Wolf-Gladrow DA (2005) Modeling the speciation and biogeochemistry of iron at the Bermuda Atlantic Time-series Study site. *Global Biogeochem Cycles* 19(1):GB1019.
6. Wiederhold JG, et al. (2006) Iron isotope fractionation during proton-promoted, ligand-controlled, and reductive dissolution of Goethite. *Environ Sci Technol* 40(12):3787–3793.
7. Bullen TD, White AF, Childs CW, Vivit DV, Schulz MS (2001) Demonstration of significant abiotic iron isotope fractionation in nature. *Geology* 29(8):699–702.
8. Beard BL, Johnson CM (2004) Fe isotope variations in the modern and ancient Earth and other planetary bodies. *Rev Mineral Geochem* 55(1):319–357.
9. Skulan JL, Beard BL, Johnson CM (2002) Kinetic and equilibrium Fe isotope fractionation between aqueous Fe(III) and hematite. *Geochim Cosmochim Acta* 66(17):2995–3015.
10. Brantley SL, Liermann L, Bullen TD (2001) Fractionation of Fe isotopes by soil microbes and organic acids. *Geology* 29(6):535–538.
11. Anbar AD (2004) Iron stable isotopes: Beyond biosignatures. *Earth Planet Sci Lett* 217(3-4):223–236.
12. Radic A, Lacan F, Murray JW (2011) Iron isotopes in the seawater of the equatorial Pacific Ocean: New constraints for the oceanic iron cycle. *Earth Planet Sci Lett* 306(1-2):1–10.


**Table S3. Iron isotope results ($\delta^{56}Fe$) for standard reference materials processed and run at similar concentrations to dissolved and particulate samples**

| Standard | Measured value ±2 SD, ‰ | Reference values,* ‰ |
|---|---|---|
| BCR-2 | 0.04 ± 0.07 ($n = 12$) | 0.03 ± 0.06 (1); 0.09 ± 0.01 (2); 0.08 ± 0.13 (3); 0.05 ± 0.08 (4); 0.09 ± 0.02 (5); 0.08 ± 0.04 (6) |
| NOD-A-1 | −0.41 ± 0.08 ($n = 9$) | −0.42 ± 0.07 (1) |
| GSI[†] | 0.34 ± 0.07 ($n = 4$) | 0.24 ± 0.10; 0.32 ± 0.06; 0.41 ± 0.04 (7) |
| GSD[†] | 0.45 ± 0.11 ($n = 5$) | 0.42 ± 0.11; 0.55 ± 0.03; 0.52 ± 0.07 (7) |

*Literature reference for values is in parentheses.

[†]GEOTRACES IC1 reference samples collected at the Bermuda Atlantic Time-series Station (BATS) intercalibration station (7).


1. Dideriksen K, Baker JA, Stipp SLS (2006) Iron isotopes in natural carbonate minerals determined by MC-ICP-MS with a 58Fe-54Fe double spike. *Geochim Cosmochim Acta* 70(1):118–132.
2. Craddock PR, Dauphas N (2011) Iron Isotopic Compositions of Geological Reference Materials and Chondrites. *Geostandards and Geoanalytical Research* 35(1):101–123.
3. Sharma M, Polizzotto M, Anbar AD (2001) Iron isotopes in hot springs along the Juan de Fuca Ridge. *Earth Planet Sci Lett* 194(1–2):39–51.
4. Dauphas N, et al. (2004) Chromatographic separation and multicollection-ICPMS analysis of iron. Investigating mass-dependent and -independent isotope effects. *Anal Chem* 76(19): 5855–5863.
5. Dauphas N, et al. (2009) Iron isotopes may reveal the redox conditions of mantle melting from Archean to Present. *Earth Planet Sci Lett* 288(1–2):255–267.
6. Weyer S, et al. (2005) Iron isotope fractionation during planetary differentiation. *Earth Planet Sci Lett* 240(2):251–264.
7. Boyle EA, et al. (2012) GEOTRACES IC1 (BATS) contamination-prone trace element isotopes Cd, Fe, Pb, Zn, Cu, and Mo intercalibration. *Limnol Oceanogr Methods* 10:653–665.